Trap-state suppression and improved charge transport in PbS quantum dot solar cells with synergistic mixed ligand treatments

Santanu Pradhan[1], Alexandros Stavrinadis[1], Shuchi Gupta[1], Yu Bi[1], Francesco Di Stasio[1], and Gerasimos Konstantatos[1,2]*

[1] ICFO-Institut de Ciencies Fotoniques, The Barcelona Institute of Science and Technology, 08860 Castelldefels (Barcelona), Spain

[2] ICREA—Institució Catalana de Recerca i Estudis Avançats, Passeig Lluís Companys 23, 08010 Barcelona, Spain

* gerasimos.konstantatos@icfo.es

Abstract

The power conversion efficiency of colloidal PbS quantum dot based solar cells is significantly hampered by lower than expected open circuit voltage (V_{OC}). The V_{OC} deficit is considerably higher in QD based solar cells compared to other types of existing solar cells due to in-gap trap induced bulk recombination of photogenerated carriers. Here, we report ligand exchange procedure based on a mixture of zinc iodide and 3-mercaptopropyonic acid to reduce the V_{OC} deficit without compromising the high current density. This layer-by-layer solid state ligand exchange treatment enhanced the photovoltaic performance from 6.62% to 9.92% with a significant improvement in V_{OC} from 0.58V to 0.66V. We further employed opto-electronic characterization, XPS and PL spectroscopy to understand the origin of V_{OC} improvement. The mixed ligand treatment reduces the sub bandgap traps and significantly reduces the bulk recombination in the devices.

1

Introduction

In recent years, tremendous development of PbS colloidal quantum dots (CQDs) based photovoltaics (PV), have made this third generation PV technology promising for commercialization [1]. Some attractive features of this technology are its spectral coverage, its compatibility with flexible substrates and with solution-based and scalable fabrication techniques. The continuous research efforts in this field have improved the solar cell power conversion efficiency (PCE) of PbS CQD cells to more than 11% in 2016 (certified PCE 11.3%) [2] from a PCE of less than 1% a decade ago[3]. This progress in device performance has been due to advanced understanding of the material properties as well as the device operation principles [4]. Understanding effects related to quantum confinement [5,6], surface passivation [7-10], band engineering [11,12], charge carrier mobility [13,14], charge collection[15,16], remote trap passivation [17,18] and carrier recombination dynamics [19,20] in CQD solids, have led to better CQD solar cells.

Despite these improvements, the PCE of these solar cells are still below the expectations with one main limiting factor being the large open-circuit voltage (V_{OC}) deficit. The V_{OC} deficit, defined as the difference between the band gap and the open circuit voltage is higher for these devices (0.55 V to 0.75 V for 1.1 to 1.4 eV band gap) [21] compared to the c-Si (0.38 V for 1.12 eV band gap), CIGS (0.35 V for 1.1 eV band gap), GaAs (0.3V for 1.42 eV band gap) and organometallic halide perovskite (0.4V for 1.5 eV bandgap) based solar cells [22]. Though the underlying reasons for this V_{OC} deficit in the case of PbS QDs solar cells are not fully understood yet, the abundance of in-gap states, introduced by the presence of unpassivated surface sites and off-stoichiometries [21, 23] of QDs, are considered the main suspects. The recent high efficiency devices using halide passivation (mainly organic iodide) show improved stability and high short-circuit current density (Jsc) around 25 mA/cm^2 mainly due to improved charge carrier mobility but the Voc is limited to half the bandgap of the QDs. In contrast, solar

cell devices with QDs passivated solely with organic ligands such as EDT, BDT, and MPA have shown higher Voc, yet they suffer from low mobility, poor charge transport and hence low PCE [8,11,24]. To reduce the amount of in-gap traps, as well as to improve charge collection, simultaneous organic and inorganic ligand treatment may be necessary as has been demonstrated by Ip et. al. [25]. In that report, the halide treatment of the QDs was performed in solution and was followed by the organic ligand treatment on the QD films during the layer-by-layer (LbL) growth.

Inspired by this approach we posited that a synergistic hybrid ligand treatment taking place simultaneously in-situ during the LbL growth of the films would offer a more balanced passivation of the surface of QDs and result in higher quality films. To implement this we decided to employ instead inorganic halide salts in order to circumvent the incompatibility challenges in mixing organic halide (such as TBAI or EMII) with organic ligands. Metal halides have been incorporated in the QD matrix using precursor solution during the synthesis [26] or using post-synthetic treatments [27]. Crisp et.al. showed reported an efficiency of 7% employing a layer-by- layer solid state metal iodide ligand treatment yet these devices suffered from lower V_{OC} and fill factor (FF) due to sub-bandgap energy states introduced through uncharged Pb or undesired contamination during the ligand exchange process[28]. Recently, Ko et.al. have showed that a short treatment of metal halide on the PbS QDs before the organic ligand treatment improved the V_{OC} by nearly 100 mV by balancing surface charge off-stoichiometry, in turn reducing the mid-gap emissive trap density, yet the resultant efficiency was approximately 7.3% due to a V_{OC} deficit of 0.72 V for 1.2 eV PbS QD[29]. These reports intrigued us to develop a layer by layer solid state ligand exchange method with mixed ligands comprising of metal iodide and organic acid to facilitate the advantages of both charge mobility improvement and trap state reduction.

Here we introduce a ligand treatment where we mix an inorganic halide (zinc iodide (ZnI_2)) with 3-mercaptopropionic acid (MPA) before applying them to the layer-by-layer ligand treatment. MPA is chosen as it helps in reducing the mid-gap states by protecting the surface from being oxidised [14]. On the other hand, ZnI_2 is chosen as the metal iodide for better charge transport and it does not form solid complexes with MPA when the two are mixed in solution. The PbS QDs were deposited over ZnO QDs to form depleted heterojunction solar cell structure with the final 2 layers treated with 1,2-Ethanedithiol (EDT) for electron blocking layer (details in experimental section). Effect of the mixed ligand treatment on the device performance compared to the ZnI_2 salt based treatment is studied thoroughly and discussed below.

Results & Discussions

Photovoltaic performance

The scanning electron microscope (SEM) cross-sectional micrographs of the ZnI_2 and ZnI_2_MPA mixed treated full devices are shown in Figures 1 (a) & (b) respectively. The optimized active layer thickness is almost the same for the two devices. We exclude the MPA treated devices performance from the subsequent discussion as they suffer from low current, high series resistance and low PCE (Supporting Figure S1) and we therefore focus on the comparison of the ZnI_2 and ZnI_2_MPA treated devices. The optimized device was achieved through mixing of MPA to 25 mmol ZnI_2 in methanol solution (0.01% (v/v)). The effect of different ZnI_2 and MPA mixing concentrations on the photovoltaic performance is summarized in supporting information (S2). The PV figures of merit for ZnI_2 and ZnI_2_MPA treated devices are summarised in Table 1. The average PCE improved from 6.34% to 9.62% when we mixed ZnI_2 solution with MPA solution whereas the champion device showed an improved PCE of 9.92% (showed in Figure 1(c)). The important factor behind the improvement of the device

efficiency comes from the improvement of both V_{OC} and J_{SC} (short-circuit current density) whereas the fill factor (FF) improved slightly due to some minor improvements in series resistance (decreased from 86.78 Ω to 76.94 Ω) and shunt resistance (increased from 16.39 kΩ to 20.30 kΩ). The most notable change is observed in the V_{OC}, which improves from 0.568 V to 0.654 V with addition of MPA to the ZnI_2 solution. To our knowledge, this is the highest V_{OC} observed in a PbS QD based depleted heterojunction solar cell with such a high J_{SC} for a 1.18 eV band gap PbS QD. Even larger V_{OC} values have been reached with smaller QDs: when their bandgap is tuned to 1.26 eV the solar cell reached 0.7 V V_{OC}. The V_{OC} dependence on QD band gap is summarized in supplementary information (S3). The results point to a reduced V_{OC} deficit of 0.5-0.6 V compared to previous reports with V_{OC} deficit of 0.6-0.8V for energy band gap ranging from 1.1 to 1.4 eV [21,30,31]. The J_{SC} also exhibited a significant rise from 19.52 mA/cm^2 to 24.37 mA/cm^2 with MPA mixing reflecting also upon the external quantum efficiency (EQE) spectra with an overall improvement throughout the wavelength region and a significant rise in the near infra-red (IR) region for ZnI_2_MPA treated device (Figure 1(d)). The stability of these devices was monitored over a period of 25 days from the device fabrication, left in air ambient conditions. The PCE improved for up to 5 days due to the initial enhancement of J_{SC} and then decreased due to the constant degradation in FF (the figures of merit are summarised in supporting information (S4)). Nevertheless, the overall PCE still remain within nearly 90% of its initial value after 25 days.

Intensity dependent V_{OC} and J_{SC} analysis

To understand the charge generation-recombination mechanism and device operation principle under light, we measured the dependence of V_{OC} and J_{SC} over an intensity range from 0.1 to 1 sun as depicted in Figure 2. The J_{SC}-suns curve shows similar intensity dependence for both ZnI_2 and ZnI_2_MPA mixed ligand treated device. The curves were fitted with the relation $J_{SC} \propto \Phi^p$, where Φ is the intensity and p is the exponent for the dependence. The calculated p factor

from both curves shows a value of 0.96. This implies that photocurrent in both devices is determined by the generation rate of electron-hole pairs due to photon absorption and not by space-charge region formed due to unbalanced charge transport of electrons and holes [32]. The major difference is observed in the suns-V_{OC} dependence for ZnI_2 and mixed ligand treated devices. The logarithmic fitting of this dependence yields the ideality factor (η) (supporting information S5). The fitting of the intensity dependent V_{OC} curve shows that η is reduced to 1.05 from 1.41 with the application of MPA mixing. This value of η ,approaching unity, is an exciting result, as most of the high efficiency depleted heterojunction solar cells with PbS QDs reported η around 1.5 [21,33,34]. The value of η in between 1 and 2 implies the presence of in-gap traps and their influence in the recombination dynamics [35, 36]. The in-gap emissive states have been identified as one of the most relevant roadblock in achieving higher V_{OC}. η close to 1 points to reduction of in-gap trap states in the QDs with ZnI_2_MPA treatment. The cleaner band-gap results in band to band recombination and reduction in trap-mediated recombination losses.

Recombination dynamics

We further employ transient photovoltage (TPV) and photocurrent (TPC) techniques in order to gain more insights and quantitative information regarding charge transport, recombination dynamics, and trap state density. Small perturbation TPV measurements directly measure charge recombination in PbS QD solar cells. The lifetime (τ) calculated from the V_{OC} decay curve with different light bias intensities is shown in Figure 3(a). The slower recombination lifetime for the ZnI_2_MPA treated device compared to ZnI_2 predicts a lower recombination loss. The recombination rate (R) (defined as the ratio between the excess carrier concentration with the pulse application and the recombination lifetime) plot vs V_{OC} gives more insight about the charge recombination dynamics (see in Figure 3(b)). The ZnI_2 treated device showed relatively higher R even at low V_{OC}. Using the TPV and TPC techniques, we try to understand

trap states in QDs according to a reported procedure [25] (details in the supporting information S6). The result showed in Figure 3(c) confirms a cleaner in-gap trap density in case of ZnI_2_MPA treated device. This direct evidence of lower in-gap state density is consistent with the evidence of improved ideality factor and lower recombination losses.

We further plot together, in Figure 3(d), the TPC behaviour of these two devices to compare the charge transport behaviour inside the devices. The ZnI_2_MPA treated device showed a much faster photocurrent transient (transit time 0.18 μs) compared to the ZnI_2 treated one (transit time 1.16 μs). This nearly 10 times acceleration in transit time indicates higher charge carrier mobility and better charge transport in ZnI_2_MPA treated QDs, consistent with the higher short-circuit current in these devices compared to ZnI_2 treated ones. A rough idea of the transit mobility can be obtained considering built-in potential (V_{bi}) as the only source of electric field assisting in the charge transport through drift [37]. V_{bi} of the devices was obtained from the Mott-Schottky plot of the capacitance voltage characteristics (Supporting information S7). V_{bi} was found to be 0.72V in ZnI_2_MPA treated device compared to 0.61V in case of ZnI_2 treated device. The calculated transit mobility was found to be increased to 3.67×10^{-3} $cm^2s^{-1}V^{-1}$ with the addition of MPA in the ligand from 6.84×10^{-4} $cm^2s^{-1}V^{-1}$. This almost 5 times improvement in mobility further corroborates the improved surface passivation enabled via the hybrid ligand passivation over the ZnI_2-only device.

X-ray photoelectron spectroscopy analysis

We further employ X-ray photoelectron spectroscopy (XPS) to correlate the physico-chemical effects of the ligand treatment on the PbS surface with the device performance and optoelectronic properties. Figure 4 shows analyzed high resolution S2p, O1s and Pb4f XPS spectra of MPA, ZnI_2 and ZnI_2_MPA treated PbS QDs. Similarly to different previous reports [8, 23, 38, 39], these spectra are deconvoluted by considering S attributed to PbS, bound and

unbound thiolates, Pb attributed to undercharged Pb, Pb-S and Pb-carboxylate, and O attributed

to Pb-O, -OH, H2O and –COO-.The S2p spectra show increased contents of bound thiolates

and suppressed presence of unbound thiolates when the hybrid ZnI_2_MPA treatment is

employed. The reduction of dangling thiolates signifies better surface passivation with mixed

ligand treatment. For O1s spectra, ZnI_2 treated QDs shows presence of atomic PbO along with

–OH which introduce sub-bandgap states. With MPA treatment, the amount of atomic O

diminished but the presence of –OH increased a lot. Cao et. al. showed device performance

degradation that is correlated with –OH presence[8] . ZnI_2_MPA treated dots showed reduction

of both atomic O and –OH from the surface, species that are associated with the formation of

traps in PbS QDs. Further, the reduction of carboxylate-Pb and metallic Pb in mixed ligand

treated device compared to the ZnI_2 treated and MPA treated devices endorse the fact of

reduction of emissive sub-band gap states as with ZnI_2 treated device undercharged Pb leads

to the formation of emissive sub-band gap [23]. We summarize the quantitative analysis of the

XPS spectra to understand the stoichiometry of the ligand treated devices in Table 1. The

overall contamination of Zn, O, C are much less in ZnI_2_MPA treated devices compared to the

ZnI_2 treated device. We attribute the presence of zinc in the films to the formation of undesired

organometallic zinc complexes, most likely zinc oleate, and not to the presence of ZnI_2. This

can be further understood by examining the Zn and I ratio of the ZnI_2 and ZnI_2_MPA treated

devices. In both ZnI_2 and ZnI_2_MPA treated samples, the I/Zn ratio is not 2 which would be

expected if zinc is attributed to unreacted ZnI_2. In fact, for the ZnI_2 treated sample, excess Zn

is observed whereas for ZnI_2_MPA treated device, I/Zn ratio is higher than 2. Therefore, we

propose that upon treating the films with ZnI_2, iodide is exchanged with oleate on the surface

of the dots and that leads to the formation organometallic zinc complexes onto the QD films.

Washing away these zinc containing impurities is greatly facilitated by the presence of MPA.

This hypothesis is further corroborated by the fact that the Zn 2p3/2 peak (supporting Figure

S6) shifts 0.3 eV for ZnI$_2$_MPA treated sample compared to ZnI$_2$ treated samples. Overall, the suppression of unwanted chemical species from the QD surface upon our mixed ligand treatment, can explain the improved optoelectronic properties and performance of the as made QD films and devices.

Photoluminescence studies

We employ photoluminescence (PL) spectroscopy to further support our claim about the reduction of emissive in-gap states with ZnI$_2$_MPA treated device. The unpassivated sites induce mid-gap states which in turn affect the PL spectra as they introduce different channels of radiative and non-radiative recombination. Figure 5(a) compares the emission intensity of ZnI$_2$ and ZnI$_2$_MPA treated mixed ligand treated PbS QDs. Massive improvement of the band-edge PL intensity was observed when QDs were treated with mixed ligand compared to only ZnI$_2$ treated ones, similar to MPA treated samples (supporting Figure S7). This suggests that with mixed ligand treatment the non-radiative emission channels are partially suppressed compared to ZnI$_2$ treated QDs. Moreover, strong emission corresponding to 0.84 eV with ZnI$_2$ treated QDs was observed (Figure 5(b)). This sub-band gap emission is a clear evidence of the presence of poorly emissive in-gap states strongly present in the case of ZnI$_2$ treated films. This sub-band gap emission was drastically supressed with the addition of MPA. The PL spectra also suggests that ZnI$_2$ treated dots have higher Urbach tail (E$_U$) energies compared to mixed ligand treated ones. To verify this, we have calculated E$_U$ from the corresponding slope of EQE spectra of the devices as described by Hages et. al.[40]. The calculated E$_U$ reduced to 23 meV for mixed ligand treated device compared to 45 meV of the ZnI$_2$ passivated device as shown in Figure 5(c). Likewise, the analytic calculation of the corresponding ideality factor [41] predicts similar kind of difference in E$_U$ (Supporting information S10). Importantly the E$_U$ is lower than room temperature thermal energy (26 meV) with mixed ligand treatment. This leads

9

to enhanced thermal de-trapping of minority carriers and thereby reduced trap assisted recombination.

Conclusions

We have shown that a mixed ligand treatment comprising hybrid inorganic metal iodide salts (ZnI_2) and organic MPA improves drastically the PV performance in PbS QD solar cells. This approach exploits the complementary benefits of inorganic ligands for improved carrier transport and robustness with those of organic ligands for improved passivation and in-gap state suppression. The synergy of the two leads to the simultaneous achievement of high Voc and Jsc and an overall PCE of nearly 10%. To elucidate the origins of the synergistic mechanisms at play we have employed a very broad range of characterization techniques to show that the hybrid passivation suppresses dramatically the presence of in-gap states and the associated recombination mechanisms thereof and has therefore led to higher performance solar cells compared to those based on either of the two ligand treatments. On a broader perspective this work paves the way towards new hybrid ligand engineering of QD solids as means to reach record performance QD solar cells.

Experimental Section

Synthesis of PbS QDs: Schlenk technique was used to synthesize PbS QDs following standard recipe. 2 mmol lead oxide (PbO), 4.7 mmol oleic acid, and 9.4 mmol 1-octadecene (ODE) were pumped overnight at 95 ^{0}C. Then 15 mL of ODE was added and the temperature of the reaction was raised to 120 ^{o}C. When this point is reached, 1 mmol hexamethyldisilathiane mixed with 10 mL ODE was quickly injected. The heating was stopped (without removing the heating mantle) and the sample allowed to cool down slowly (~1 hour). The NCs were isolated by adding acetone and then centrifuging, purified by dispersion/precipitation with toluene/acetone

3 times, and finally dispersed in anhydrous toluene. The obtained QDs were further treated with n-butylamine ligand for 1 day in the glove box and then cleaned with methanol. The final QDs were dispersed in anhydrous toluene (30 mg ml^{-1}) before applying for the device formation.

Photovoltaic device fabrication: ITO coated glass substrates were cleaned thoroughly with soap water and acetone respectively before boiling in 2-propanol for 10 min. Then the substrates were dried using nitrogen gun prior to material deposition. ZnO nanocrystals were prepared using the standard method reported elsewhere [17]. The concentration of the prepared ZnO nanocrystal colloidal solution in chloroform was fixed at 45 mg ml^{-1}. For ZnO bottom layer formation, the cleaned ITO coated substrates were fully covered with ZnO nanocrystal solution and were immediately spun at 3500 rpm for 30 sec. The substrates were then shifted to a hotplate with pre-set temperature of 250 ^{0}C and left for 30 min to bake. After that, the heat source was switched off and the substrates were allowed to cool down to room temperature. The active layer of the device was formed by sequential layer by layer spin coating technique. For a single layer, cleaned PbS solution in anhydrous toluene (30 mg ml^{-1} concentration) was employed on the ZnO covered substrate and spun immediately with 2500 rpm for 15 sec. Then the rotation was stopped before applying 5 drops of ZnI_2 (25 mM in methanol) or ZnI_2_MPA mixed ligand (25 mM ZnI_2 with 0.01% MPA (v/v) in Methanol) solution to the PbS layer and waited 5 sec for the ligand exchange. After that, the rotation was started immediately to dry the sample for 10sec. Then the unreacted ligands were washed twice with few drops of methanol solution and the film was dried with 10 sec more rotation. The process was repeated for 12 times to get a thicker film. The final 2 layers were formed with EDT treatment. The PbS layer was treated with 0.02% EDT in acetonitrile for 30 sec and then was rotated for 10 sec to dry it before washed it twice with few drops of acetonitrile solution. The as synthesized films were kept in the glovebox for overnight prior to the metal electrode deposition. Au metal was

deposited in a Kurt J. Leskar Nano 36 system at a rate of 2 Å S^{-1} for the final thickness of 150 nm. The active device area was determined by a circular shadow mask of 2 mm diameter. After the electrode deposition, the devices were transferred to glovebox to anneal at 80°C on a pre-heated hotplate for 5 minutes. The devices were taken out of the glovebox and stored in air for further characterizations.

Photovoltaic performance characterization: All the PV characterizations were performed in ambient conditions. The device I-V responses were performed using a Keithley 2400 source meter. Illumination intensity of AM 1.5 was maintained using a class AAA solar simulator (Oriel sol3A, Newport Corporation). The accuracy of the measurement was determined as ±4%.

EQE measurements: EQE measurements were performed with an in-house build experimental set-up by using chopped (220 Hz, Thorlab) monochromatic illumination. The power was measured with a calibrated Newport-UV power meter. The device response of the chopped signal was measured using a Stanford Research system lock-in amplifier (SR830) which was fed by a Stanford Research system low noise current pre-amplifier (SR570). The final EQE spectra were obtained with the help of LabVIEW program.

Intensity dependent V_{OC} and J_{SC} measurements: The intensity depended V_{OC} and J_{SC} were measured with a LED lamp calibrated with Newport 818-UV power meter and an Agilent 4000X oscilloscope. The intensity of the lamp was varied with the DC applied bias from the function generator of the oscillator. The voltage was recorded on the oscilloscope with input impedance 1 MΩ and the current with 50 Ω. The accuracy of this measurement was estimated to be within ±8%.

Transient photovoltage and photocurrent techniques: Transient photovoltage (TPV) and photocurrent (TPC) of the devices were measured with an in-house-built set-up. The set-up

comprises a LED lamp to provide steady state white bias light, a 637 nm wavelength laser (Vortran Stradus) and an Agilent 4000X oscilloscope. The LED lamp was used to get steady V_{OC} of the device. The intensity of the lamp was controlled by the external applied DC bias and was attenuated with metal-mesh according to the necessity. The laser was controlled by the function generator with a frequency of 10 Hz and pulse width of 100 μs. The intensity of the laser was controlled to keep the voltage transient amplitude under 5% of the steady state light bias. The oscilloscope records the data using 1 MΩ input impedance for the TPV measurement and 50 Ω for TPC measurement. The V_{OC} decay curves were fitted with exponential decay to find the recombination time. The TPC curve was integrated to get the charge generated (ΔQ) in the devices due to the laser pulse. The capacitance (C) was calculated from the C= $\Delta Q/\Delta V_{OC}$ relation. The total charge carrier was calculated from the integration of C vs V_{OC} plot. Charge carrier density was calculated by dividing the total charge carriers with the device volume.

X-ray photoelectron spectroscopy measurements: XPS experiments were performed in a PHI 5500 Multitechnique System with a monochromatic X-ray source (Aluminium Kα line of 1486.6 eV energy and 350 W power), placed perpendicular to the analyser axis and calibrated using the 3d5/2 line of Ag with a full width at half maximum (FWHM) of 0.8 eV. All measurements were performed in ultra-high vacuum chamber with pressure between 5×10^{-9} and 2×10^{-8} torr. The samples were prepared with layer-by-layer method described above and each of them are with 5 layers. The collected data were processed with XPSPEAK41 software for quantitative analysis. The deconvolution of the XPS spectra was performed by fitting a sum of Lorentzian-Gaussian functions (always with 80% Gaussian weighting) to the experimental data. For consistency, the full-width-at half-maximum (FWHM) of all Gaussian-Lorentzian functions for the same spectral regions and peaks of different samples was kept the same.

Photoluminescence measurements: Photoluminescence measurements were carried out using a Horiba Jobin Yvon iHR550 Fluorolog system along with a Hamamatsu R5509-73 photomultiplier tube detector. Samples were excited with a 637 nm laser (Vortran Stradus). The acquired raw data was processed first subtracting the dark counts and normalised with respect to the absorption peak of the corresponding films.

References

(1) E. H. Sargent, *Nat. Photonics*, **2012**, *6*, 133.

(2) M. Liu, O. Voznyy, R. Sabatini, F. P. G. de Arquer, R. Munir, A. H. Balawi, X. Lan, F. Fan, G. Walters, A. R. Kirmani, S. Hoogland, F. Laquai, A. Amassian, E. H. Sargent, *Nat. Mater.* **2016** (DOI: 10.1038/nmat4800).

(3) S. a McDonald, G. Konstantatos, S. Zhang; P.W. Cyr, E.J.D. Klem, L. Levina, E.H. Sargent, *Nat. Mater.* **2005**, *4*, 138.

(4) G.H. Carey, A.L. Abdelhady, Z. Ning, S.M. Thon, O.M. Bakr, E.H. Sargent, *Chem. Rev.* **2015**, *115*, 12732.

(5) D.V. Talapin, C.B. Murray, *Science* **2005**, 310, 86.

(6) P.R. Brown, D. Kim, R.R. Lunt, N. Zhao, M.G. Bawendi, J.C. Grossman, V. Bulovic *ACS Nano* **2014**, *8*, 5863.

(7) G. H. Carey, L. Levina, R. Comin, O. Voznyy, E. H. Sargent, *Adv. Mater.*, **2015**, *27*, 3325.

(8) Y. Cao, A. Stavrinadis, T. Lasanta, D. So, G. Konstantatos, *Nat. Energy*, **2016**, *1*, 16035.

(9) X. Lan, O. Voznyy, A. Kiani, F. P. G. Arquer, A. S. Abbas, G.-H. Kim, M. Liu, Z. Yang, G. Walters, J. Xu, M. Yuan, Z. Ning, F. Fan, P. Kanjanaboos, I. Kramer, D. Zhitomirsky, P. Lee, A. Perelgut, S. Hoogland, E. H. Sargent, *Adv. Mater.,* **2016**, *28*, 299.

(10) S.M. Thon, A.H. Ip, O. Voznyy, L. Levina, K.W. Kemp, G.H. Carey, S. Masala, E.H. Sargent ACS nano, **2013**, *7*, 7680.

(11) C.-H. M. Chuang, P.R. Brown, V. Bulovic, M.G. Bawendi, *Nat. Mater*, **2014**, *13*, 796.

(12) Z. Ning, O. Voznyy, J. Pan, S. Hoogland, V. Adinolfi, J. Xu, M. Li, A. R. Kirmani,J.-P. Sun, J. Minor, K. W. Kemp, H. Dong, L. Rollny, A. Labelle, G. Carey, B. Sutherland, I. Hill, A. Amassian, H. Liu, J. Tang, O. M. Bakr, E. H. Sargent, Nat. Mater., **2014**, *13*, 822.

(13) Y. Liu, M. Gibbs, J. Puthussery, S. Gaik, R. Ihly, H. W. Hillhouse, M. Law, *Nano Lett.* **2010**, *10*, 1960.

(14) K. S. Jeong, J. Tang, H. Liu, J. Kim, A. W. Schaefer, K. Kemp, L. Levina, X. Wang, S. Hoogland, R. Debnath, L. Brzozowski, E. H. Sargent, J. B. Asbury, *ACS Nano*, **2012**, *6*, 89.

(15) X. Lan, S. Masala, E.H. Sargent, *Nat. Mater.,* **2014**, *13*, 233.

(16) Z. Jin, M. Yuan, H. Li, H. Yang, Q. Zhou, H. Liu, X. Lan, M. Liu, J. Wang, E. H. Sargent, Y. Li, *Adv. Func. Mater.,* **2016**, *26*, 5284.

(17) A. K. Rath, M. Bernechea, L. Martnez, F. P. G. Arquer, J. Osmond, G. Konstantatos, *Nat. Photonics*, **2012**, *6*, 529.

(18) A. K. Rath, F.P.G.Arquer, A. Stavrinadis, T. Lasanta, M. Bernechea, S.L. Diedenhofen, G. Konstantatos, *Adv. Mater*, **2014**, *26*, 4741.

(19) M. Graetzel, R. A. J. Janssen, D. B. Mitzi, E. H. Sargent, *Nature,* **2012,** *488*, 304.

(20) M. Yuan, O. Voznyy, D. Zhitomirsky, P. Kanjanaboos, E.H. Sargent, *Adv. Mater.,* **2015**, *27*, 917.

(21) C.-H. M. Chuang, A. Maurano, R. E. Brandt, G. W. Hwang, J. Jean, T. Buonassisi, V. Bulovic, M.G. Bawendi, *Nano Lett.,* **2015**, *15*, 3286.

(22) M. A. Green, K. Emery, Y. Hishikawa, W. Warta, E. D. Dunlop, *Prog. Photovoltaics*, **2016**, *24*, 905

(23) G. W. Hwang, D. Kim, J. M. Cordero, M. W. B. Wilson, C.-H. M. Chuang, J. C. Grossman, M. G. Bawendi, *Adv. Mater*, **2015**, *27*, 4481.

(24) Z. Ning, Y. Ren, S. Hoogland, O. Voznyy, L. Levina, P. Stadler, X. Lan, D. Zhitomirsky, E. H. Sargent, *Adv. Mater.*, **2012**, *24*, 6295.

(25) A. H. Ip, S. M. Thon, S. Hoogland, O. Voznyy, D. Zhitomirsky, R. Debnath, L. Levina, L. R. Rollny, G. H. Carey, A. Fischer, K. W. Kemp, I. J. Kramer, Z. Ning, A. J. Labelle, K. W. Chou, A. Amassian, E. H. Sargent, *Nat. Nanotechnol.*, **2012**, *7*, 577.

(26) J. Zhang, J. Gao, E. M. Miller, J. M. Luther, M. C. Beard, *ACS Nano*, **2013**, *8*, 614.

(27) D. Zhitomirsky, O. Voznyy, L. Levina, S. Hoogland, K. W. Kemp, A. H. Ip, S. M. Thon, E. H. Sargent, *Nat. Coumn.*, **2014**, *5*, 3803.

(28) R.W. Crisp, D. M. Kroupa, A. R. Marshall, E.M. Miller, J. Zhang, M. C. Beard, J. M. Luther, *Sci. Rep*, **2015**, *5*, 9945.

(29) D.-K. Ko, A. Maurano, S. K. Suh, D. Kim, G. W. Hwang, J. C. Grossman, V. Bulovic, M. G. Bawendi, *ACS Nano*, **2016**, *10*, 3382.

(30) W. Yoon, J.E. Boercker, M.P. Lumb, D. Placencia, E.E. Foos, J.G. Tischler, *Sci. Rep.,* **2013**, *3*, 2225.

(31) A. G. Pattantyus-Abraham, I. J. Kramer, A. R. Barkhouse, X. Wang, G. Konstantatos, R. Debnath, L. Levina, I. Raabe, M. K. Nazeeruddin, M. Gratzel, E. H. Sargent, *ACS Nano*, **2010**, *4*, 3374.

(32) N. Zhao, T. P. Osedach, L.-Y. Chang, S. M. Geyer, D. Wanger, M. T. Binda, A. C. Arango, M. G. Bawendi, V. Bulovic, *ACS Nano*, **2010**, *4*, 3743.

(33) D. Bozyigit, V. Wood, *J. Mater. Chem. C*, **2014**, *2*, 3172.

(34) Z. Sun, G. Sitbon, T. Pons, A. A. Bakulin, Z. Chena, *Sci. Rep.,* **2015**, *5*, 10626.

(35) T. Kirchartz, F. Deledalle, P. S. Tuladhar, J. R. Durrant, J. Nelson, *J. Phys. Chem. Lett.* **2013**, *4*, 2371.

(36) V. Malgras, G. Zhang, A. Nattestad, T. M. Clarke, A. J. Mozer, Y. Yamauchi, J. H. Kim, *ACS Appl. Mater. Interfaces*, **2015**, *7*, 26455.

(37) Y. Shao, Z. Xiao, C. Bi, Y. Yuan, J. Huang, *Nat. Comun.*, **2014**, *5*, 5784.

(38) J. M. Luther, M. Law, Q. Song, C. L. Perkins, M. C. Beard, A. J. Nozik, *ACS Nano*, **2008,** *2*, 271.

(39) V. Malgras, A. Nattestad, Y. Yamauchi, S. X. Doua, J. H. Kim, *Nanoscale*, **2015**, *7*, 5706.

(40) C. J. Hages, N. J. Carter, R. Agrawal, *J. Appl. Phys.* **2016**, *119*, 014505.

(41) T. Kirchartz, J. Nelson, *Phys. Rev. B*, **2012**, *86*, 165201.

Tables

Devices	V_{OC} (V)	J_{SC} (mA/cm^2)	FF	Efficiency (%)	R_s (Ω)	R_{sh} (kΩ)
ZnI$_2$ treated	0.568±0.006 (0.58)	19.52±0.30 (19.7)	0.572±0.010 (0.58)	6.34±0.16 (6.62)	86.78±5.01	16.39±3.16
ZnI$_2$_MPA treated	0.654±0.005 (0.66)	24.37±0.18 (24.48)	0.603±0.007 (0.613)	9.62±0.23 (9.92)	76.94±3.57	20.30±2.69

Table 1: Summary of photovoltaic figures of merit for ZnI$_2$ and mixed ligand treatments. The values in brackets indicate champion device.

Elements	Species	MPA	ZnI$_2$	ZnI$_2$_MPA
Pb	total	1.00	1.00	1.00
	Pb-S	0.85	0.85	0.88
	COO:Pb	0.13	0.09	0.09
	Metallic Pb	0.02	0.06	0.03
S	total	1.02	0.54	0.87
	S_PbS	0.60	0.54	0.59
	S_bound thiol	0.13	0.00	0.23
	S_unbound thiol	0.29	0.00	0.05
O	total	0.78	2.36	0.79
	O_PbO	0.00	0.21	0.00
	O_OH	0.70	0.60	0.08
	O_COOH	0.08	1.41	0.61
	O_H$_2$O	0.00	0.16	0.1
C		3.91	10.29	4.19
I		0.00	0.96	0.83
Zn		0.00	1.27	0.31

Table 2: Stoichiometry of MPA, ZnI$_2$, and ZnI$_2$_MPA mixed ligand treated samples, based on quantitative analysis of S2p, Pb4f, I3d, Zn2p3/2, O1s, C1s XPS spectra.
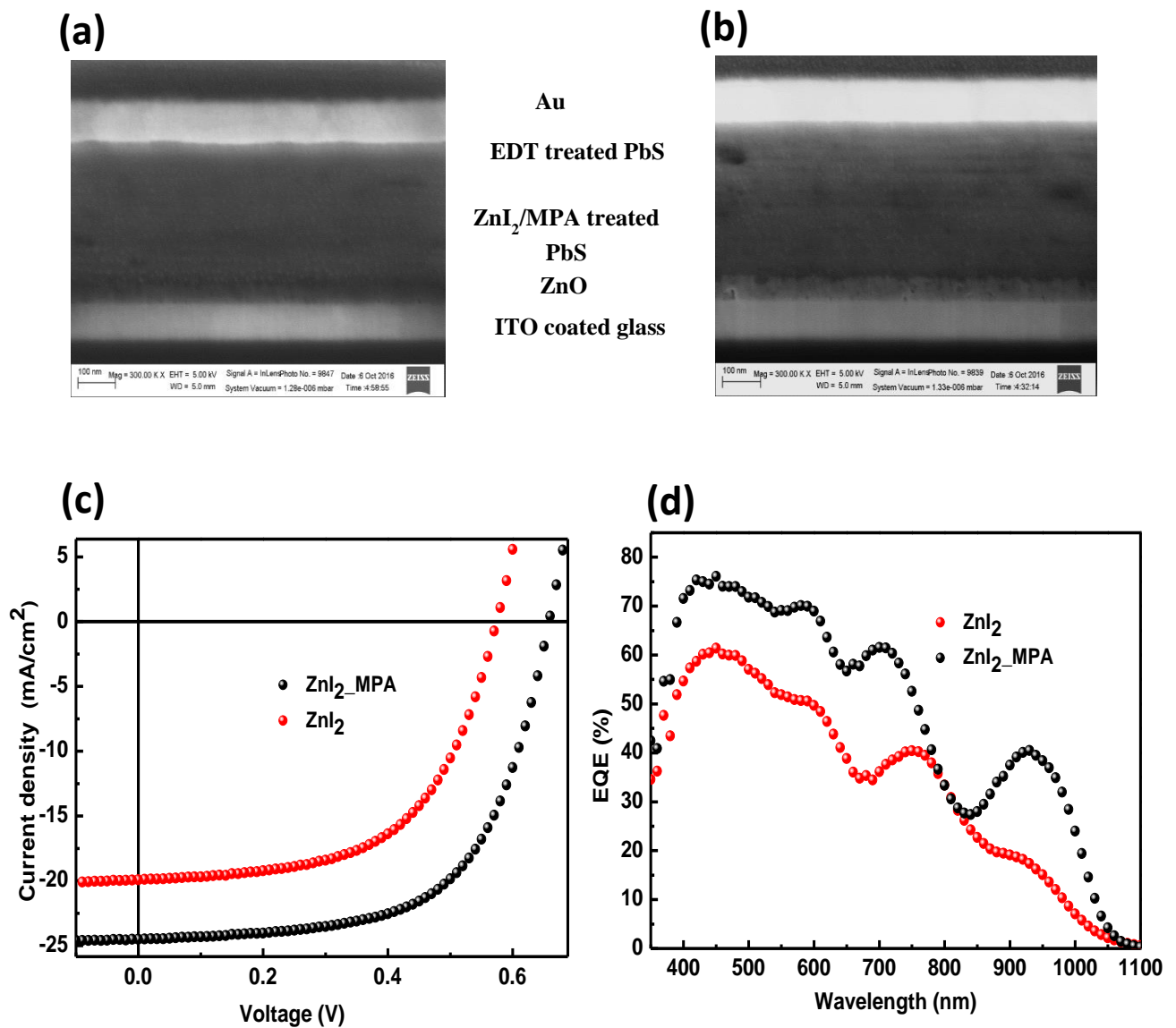
Figures

Figure 1: FIB cross-sectional images of (a) ZnI_2 treated and (b) ZnI_2_MPA treated PbS QD device. (c) Current density-voltage characterizations for the PV devices to calculate efficiency. (d) EQE spectra of the ZnI_2 and ZnI_2 mixed with MPA treated devices.
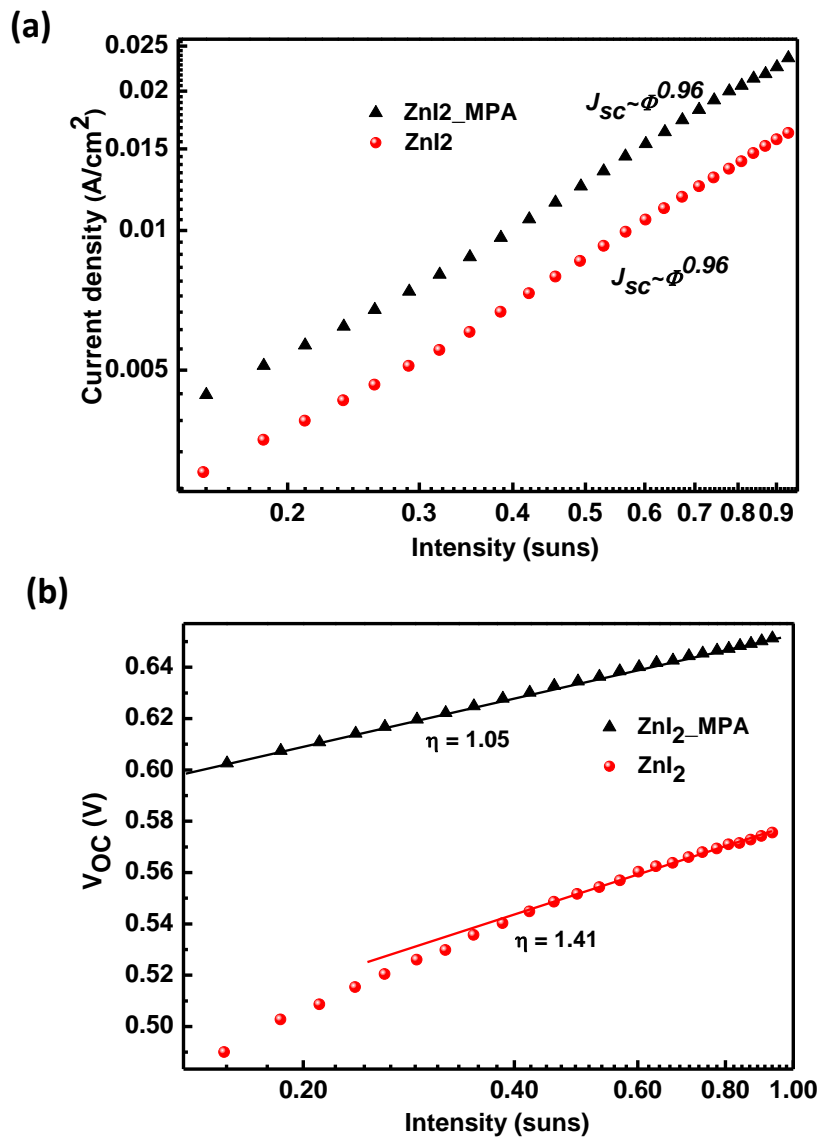
(a)

(b)

Figure 2: Intensity dependent (a) current density and (b) V_{OC} variation for ZnI_2 and mixed ligand treated PV devices.
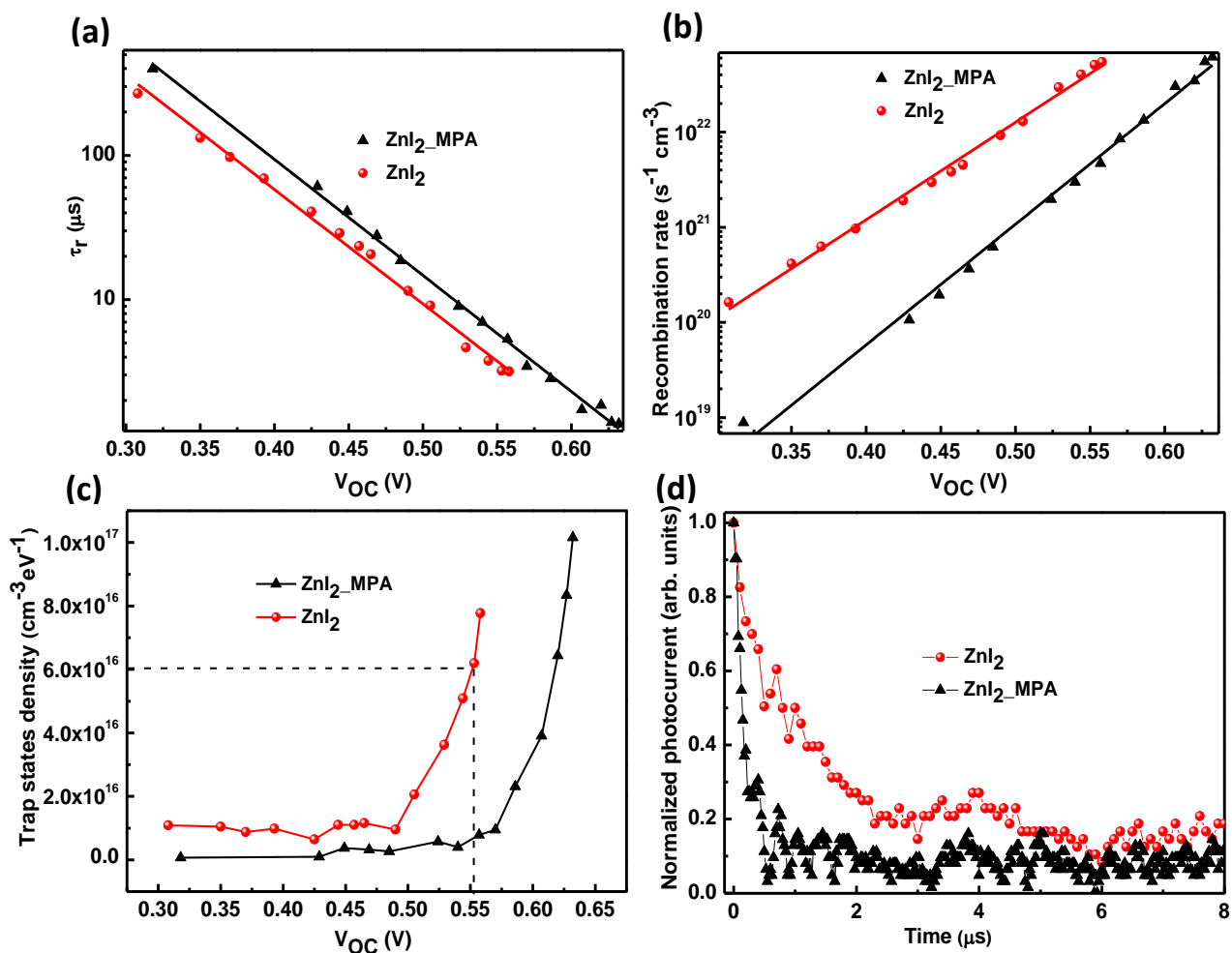
Figure 3: Comparison of the (a) recombination lifetimes, (b) recombination rate, (c) mid-gap trap density, (d) photo-current transient at short-circuit condition of ZnI_2 and ZnI_2_MPA mixed ligand treated devices. All the comparisons shows the reduction of mid-gap trap states and improvement of recombination loss for ZnI_2_MPA treated device.
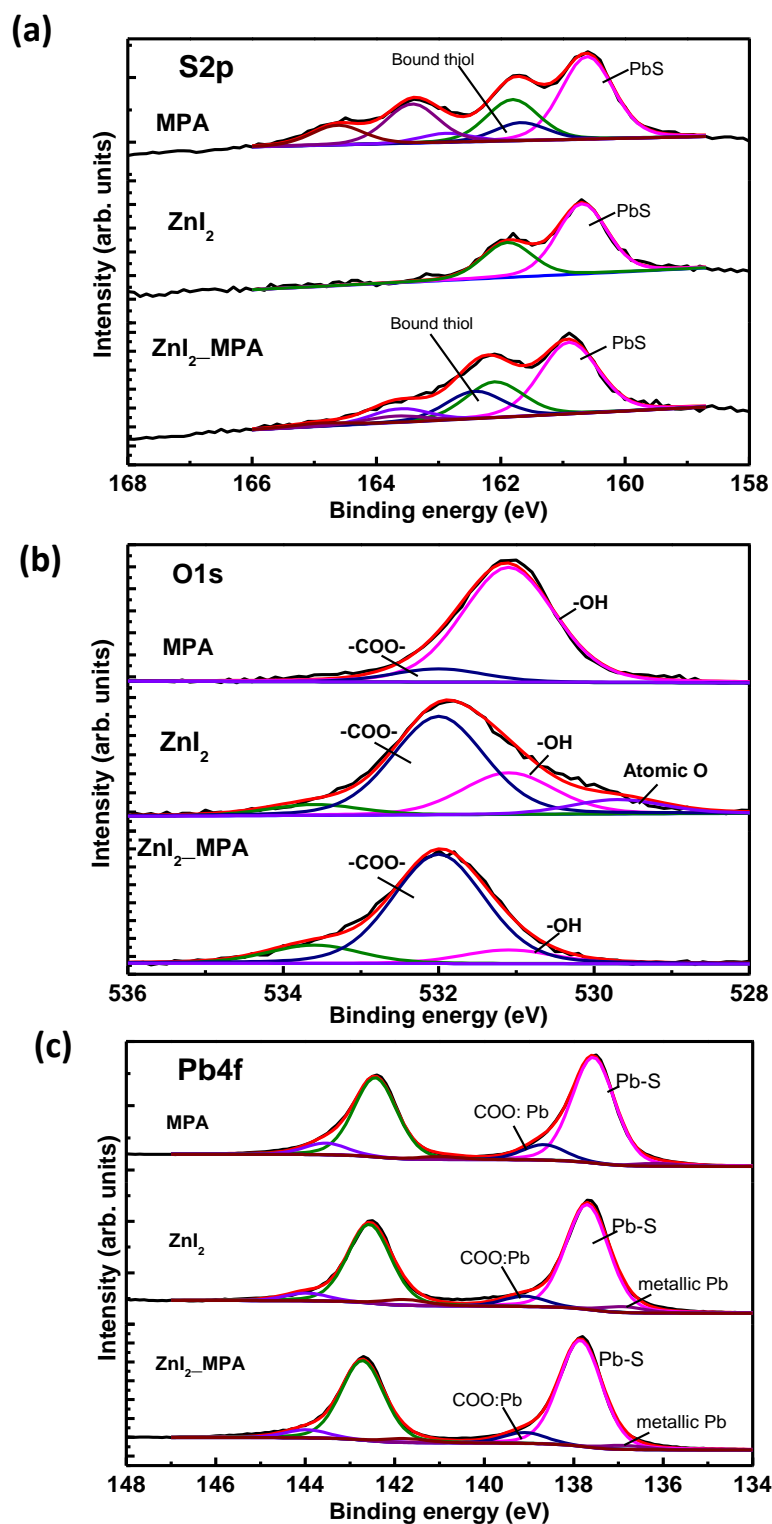
Figure 4: Deconvoluted (a) S2p, (b) O1s, (c) Pb4f XPs spectra of MPA, ZnI_2, and ZnI_2_MPA treated QD layers. With ZnI_2_MPA treatment, Pb-OH, atomic O, metallic Pb reduced whereas the bound thiol increased leading to better surface passivation.
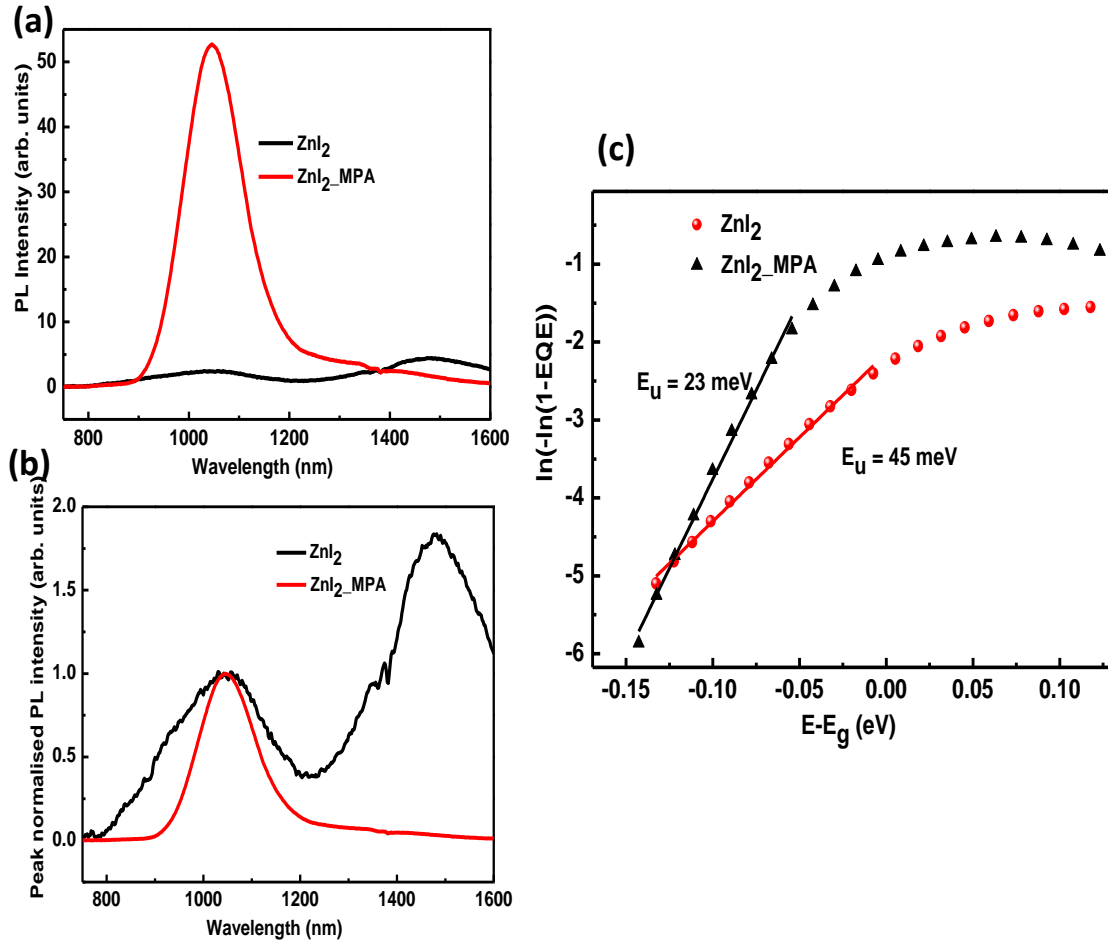
Figure 5: (a) PL intensity normalized to the absorption of the film for ZnI_2 and ZnI_2_MPA ligand treated films. There is a huge improvement in the band-edge emission in case of ZnI_2_MPA treated film. (b) Peak normalised PL intensity shows dominating sub-band gap emission in case of ZnI_2 treated films. With MPA mixing with ZnI_2 treatment, the mid-gap trap emission reduced. (c) Urbach tail energy (E_U) calculated from the EQE spectrum of the PV devices. Significant E_U reduction observed in case of mixed ligand treatment which is consistent with the PL spectra.

TOC